Planar Reflection Grating Wavelength Filters in Silicon

B. J. Luff, V. Tsatourian, P. A. L. Stopford, S. W. Roberts, J. P. Drake, S. A. Fuller, and M. Asghari

***Abstract*—The design, fabrication, and performance of reflection-type multiplexers and demultiplexers in the silicon-on-insulator material system is discussed. These devices provide a more compact alternative to arrayed waveguide grating filters in planar technologies. Their suitability for application to both dense wavelength-division multiplexing and coarse wavelength-division multiplexing optical communication systems is considered.**

***Index Terms*—Gratings, integrated optics, optical waveguides, silicon-on-insulator (SOI) technology.**

I. Introduction

WAVELENGTH filters are an essential component in modern long-haul and metropolitan optical fiber communication systems. The need to lower system costs is driving a trend toward the increased integration of optical devices into more compact subsystems with higher functionality. Waveguide-based integrated-optical technologies are being developed to address this requirement. Recently, high-functionality multiplexer variable optical attenuator (VOA) subsystems have been developed based on the silicon-on-insulator (SOI) integrated optical material system [1]. These devices use arrayed waveguide grating (AWG) filters integrated onto the same chip as solid-state VOAs.

The anticipated need for greater compactness has led to a great deal of effort on alternative filter structures to the AWG on planar technology platforms, notably the silica and InP-based waveguide systems. References [2] and [3] both consider echelle-type planar gratings and achieve significant reductions in size over equivalent AWGs. In this paper, we report on results for an alternative reflection-type filter to the echelle with grating and focusing elements based on total internal reflection. This arrangement eliminates the need for reflective coatings and hence reduces fabrication complexity. Similar reflection-transmission grating devices have also been demonstrated in InGaAsP/InP [4], polymer [5], and silica-on-silica waveguide systems [6].

II. Operating Principle

The efficiency of conventional reflection-type grating designs when used with total internal reflection is limited severely by geometrical constraints, in that a significant proportion of the light incident on the grating is lost due to the incident angle being far from normal. This loss mechanism is avoided by the transmission-reflection grating geometry of Fig. 1, where, if the grating elements are fabricated perfectly, all the light from the collimated beam is scattered in the same direction after being incident on the grating. The loss due to scattering into higher diffraction orders can be minimized by careful design, and can be made negligible for most applications. Parabolic collimating mirrors and grating elements are formed by deep etches into the silicon slab region. Total internal reflection occurs at the mirror surfaces provided the angle of incidence of the light is greater than the critical angle, which for a silicon/air interface is approximately 16.8°. Careful optical design is required to ensure the critical angle condition is met at every reflecting surface. This constraint limits the set of possible geometric arrangements.

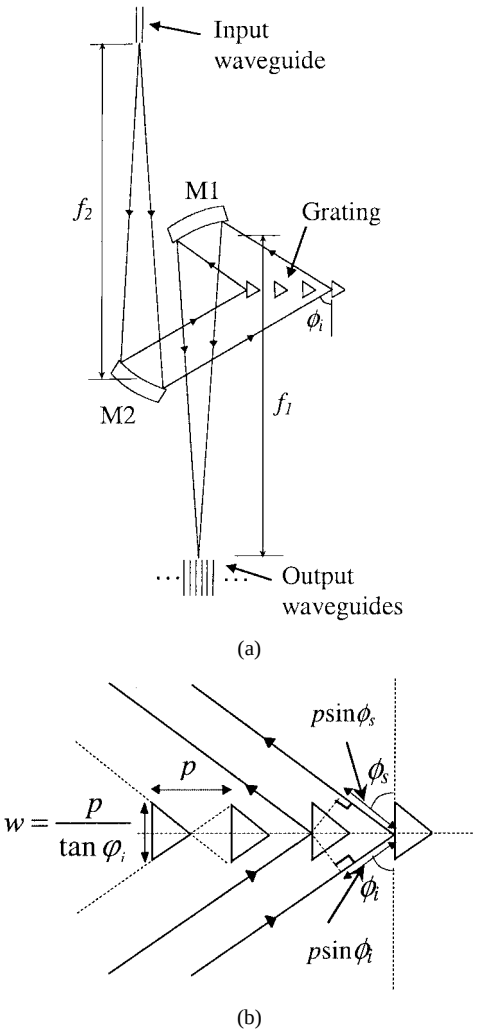

Fig. 1. Reflection demultiplexer configuration. (a) General layout. (b) Detail of the grating.

Manuscript received March 24, 2003; revised August 11, 2003.

The authors are with Bookham Technology, Abingdon, OX14 4RY Oxfordshire, U.K. (e-mail: jonathan.luff@bookham.com).

Digital Object Identifier 10.1109/JLT.2003.820046

Greater design flexibility may be provided by metal coating the mirror elements, hence allowing near-normal incidence, but at the expense of increased fabrication complexity and possibly greater polarization dependence. All designs reported here are based on total internal reflection.

Measurements on paired mirror structures indicate that the loss due to scattering and mode conversion at a parabolic mirror element is less than 0.25 dB. The most significant loss mechanism is likely to be scattering at the corners of the grating elements due to rounding caused by fabrication limitations.

A. Grating Equation, Dispersion, and FSR

Collimated light from the input parabolic mirror M2 is incident on the grating. Referring to Fig. 1, the grating equation may be written as

$$p\sin\phi_i + p\sin\phi_s = \frac{O\lambda}{n_e(\lambda)} \tag{1}$$

where p is the grating period; $\phi_{\rm i}$ and ϕ_s are the incident and scattered ray angles, respectively; O is the grating order; λ is the wavelength; and $n_e(\lambda)$ is the effective index of the waveguide mode. The center wavelength is given by

$$\lambda_c = \frac{n_e \Delta L}{O} \tag{2}$$

where ΔL is the path length difference for the center ray

$$\Delta L = 2p\sin\phi_i. \tag{3}$$

The angular dispersion of the grating is obtained by differentiating (1) to obtain

$$\frac{d\phi_s}{d\lambda} = \frac{O\left(1 - \frac{\lambda}{n_e}\frac{dn_e}{d\lambda}\right)}{n_e p\cos\phi_s}. \tag{4}$$

For small differences in wavelength, we can make the approximation $\cos\phi_{\rm s} \approx \cos\phi_{\rm i}$ and write

$$\Delta\phi_s = \frac{On_g\Delta\lambda}{{n_e}^2 p\cos\phi_i} \tag{5}$$

where n_g is the *group index*

$$n_g = n_e\left(1 - \frac{\lambda}{n_e}\frac{dn_e}{d\lambda}\right). \tag{6}$$

The waveguide dispersion $(dn_e/d\lambda)$ is determined by calculating the effective index of the fundamental mode at each wavelength. Equation (5) gives the deviation in ray angle for a change in wavelength of $\Delta\lambda$ from a specified center wavelength $\lambda_{\rm c}$.

Combining (4), (2), and (3), we see that the angular dispersion is independent of the grating period and depends only on the incidence angle and the ratio of the group index to the effective index

$$\frac{d\phi_s}{d\lambda} = \frac{2\tan\phi_i}{\lambda_c}\left(\frac{n_g}{n_e}\right). \tag{7}$$

Light from the grating is refocused by the parabolic output mirror M1. The position of output waveguide i, transmitting a wavelength spectrum centered at λ_i may be determined by straightforward geometrical ray tracing using (5). The spatial dispersion is given by

$$\frac{ds}{d\lambda} = f_1\frac{d\phi_s}{d\lambda} \tag{8}$$

where ds represents the displacement along the focal line and f_1 is the focal length of M1.

The phase change over one path length increment is given by

$$\theta = \frac{2\pi n_e \Delta L}{\lambda} \tag{9}$$

and therefore

$$\frac{d\theta}{d\lambda} = -\frac{2\pi\Delta L n_g}{\lambda^2}. \tag{10}$$

The free spectral range (FSR) for a given center wavelength can be calculated by determining the wavelength shift for which the phase change over a path-length difference is equal to 2π

$$-\frac{2\pi\Delta L n_g \Delta\lambda_{\rm FSR}}{{\lambda_c}^2} = -2\pi \Rightarrow \Delta\lambda_{\rm FSR} = \frac{\lambda_c}{O}\frac{n_e}{n_g} \tag{11}$$

i.e., the FSR is dependent on a modified order number.

B. Focusing Elements

The aperture of the mirror M2 is calculated by approximating the field distribution of the light from the input waveguide to a Gaussian profile with the $1/e$ width ω_c. The value of ω_c is related to the waveguide width at the start of the slab waveguide (free propagation) region. The validity of this approximation has been confirmed for some input waveguide widths by far-field measurements. The $1/e$ width ω of the field distribution at M2 after the light has propagated a distance z into the slab waveguide is given by [7]

$$\omega = \sqrt{\frac{4{f_2}^2 + {k_c}^2{\omega_c}^4}{{k_c}^2{\omega_c}^2}} \tag{12}$$

where $k_c = 2\pi n_e/\lambda_c$ and f_2 is the focal length of the mirror. The aperture of the mirror M1 is greater than that of M2 by a factor that takes into account the angular dispersion (5).

III. Results

Ridge waveguide devices were fabricated by dry-etching of SOI material. The start thickness of the epitaxial silicon layer was 5 μm. This layer thickness was used so that large-area single-mode ridge waveguides could be fabricated that may be interfaced with low loss to standard single-mode optical fibers using an existing mode-converting taper technology [8]. One consequence of the ridge waveguide dimensions chosen is that the planar slab region containing the mirrors and grating elements is multimode at wavelengths in the region of 1.5 μm. However, excitation of higher order modes at the ridge waveguide/planar region interface may be reduced to an acceptable level by tapering the ridge waveguide laterally. Of greater concern for using a multimode slab region is excitation of higher order modes at mirror and grating elements, or at the interface with an etched birefringence compensation region, as discussed below. However, a thinner guiding layer would lead to increased

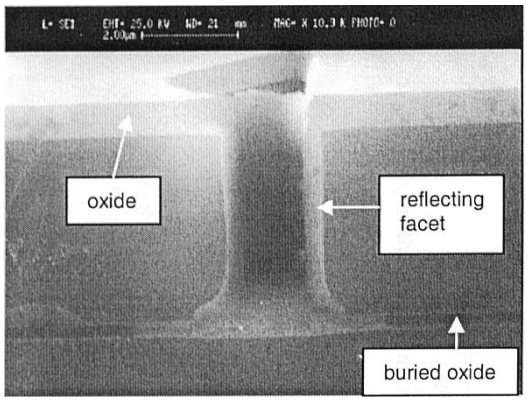

Fig. 2. SEM image of a section through a triangular etched grating element. Undercutting is occurring at the base of the element.

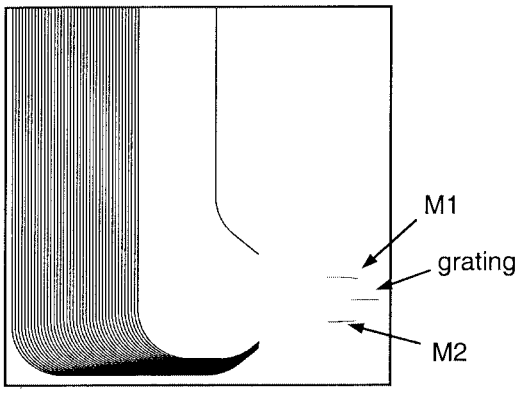

Fig. 3. Multiplexer chip layout. Chip dimensions are 33×33 mm^2.

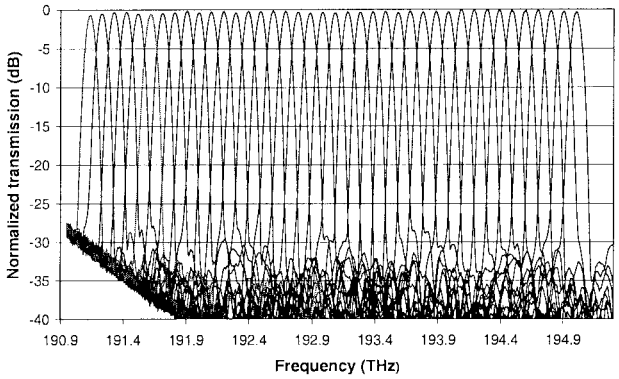

Fig. 4. Normalized output spectra for the 40-channel 100-GHz channel spacing multiplexer device shown in Fig. 3.

birefringence and make interfacing to standard fiber more difficult.

Mirror elements were formed by deep-etching to the buried oxide. Fig. 2 shows a scanning electron microscope (SEM) cross-section of a typical triangular grating element. This image shows some undercutting at the base of the element, which will have the effect of introducing loss into the structure and also contribute crosstalk due to excitation of higher order slab modes.

Typical waveguide lateral dimensions were 8–10 μm at the input to the slab region and at the focal line. The waveguides then taper to normal single-mode dimensions (3–4 μm). The tapering is present for two reasons: to minimize coupling between the output guides and to ensure good coupling to the slab.

Spatial mode filtering introduced into the output fanout was found to lower adjacent channel crosstalk. This effect is likely to be due to higher order slab modes excited at the mirrors coupling into the output guides. The form of filtering found to be most effective was the introduction of a 90° turn into the output fan-out.

A. DWDM Devices

The chip layout of a 40 channel multiplexer is shown in Fig. 3. The chip size was 33×33 mm; the bend radius was 4 mm and long straight waveguides were included on the input and outputs to allow for possible integration of solid-state VOA elements. If this integration is not required, the chip length in one dimension may be reduced by a factor of two. Output waveguide pitch was 250 μm.

Fig. 4 shows typical output spectra for the 40-channel multiplexer device of Fig. 3. The channel spacing was 100 GHz. The on-chip insertion loss (i.e., not including fiber–chip interfaces) at the center channel peak was typically 5 dB. This includes 1 dB due to the method used to broaden the Gaussian peaks to achieve a wide bandwidth: in this case, the input waveguide was simply widened with respect to the output waveguides. The rise in the noise floor is due to the significant dropoff, at the low-frequency end, of the power output of the broadband source used for the measurement.

As mentioned earlier, the loss due to a single reflection at a parabolic mirror element is expected to be 0.25 dB. The most significant contribution to the excess loss is expected to be the grating itself, a result of fabrication limitations such as the undercut features seen in Fig. 2, rounding of the triangle corners, and facet verticality. Improvements to lithography and etch processes are expected to reduce the excess loss considerably. The typical fiber–chip single interface loss achieved for SOI devices using vertical mode transformers is 0.5 dB [8].

The polarization dependent loss (PDL) at the channel centers was less than 0.5 dB. However, the polarization dependent frequency (PDF) was 20 GHz: this compares well with the value of 22 GHz expected due to the fundamental geometric birefringence of the slab waveguide region, as given by

$$\Delta f = f \frac{\Delta n}{n_{\mathrm{TE}}} \tag{13}$$

where f is the frequency, Δn is the birefringence of the slab, and n_{TE} is the TE effective index of the slab

This value of PDF is unacceptable for many applications. One possible technique of PDF reduction is that described in [9], where a shallow-etched birefringence compensating region is introduced into the light path. Fig. 5 illustrates the application of this technique to the reflection-transmission grating considered here.

The geometry of the shallow etched region is defined by

$$c_i - c_0 = \frac{i \Delta L \Delta n'}{2(\Delta n - \Delta n')} \tag{14}$$

where Δn is the birefringence of the unetched slab and $\Delta n'$ is the birefringence of the shallow-etched region. Forty-channel

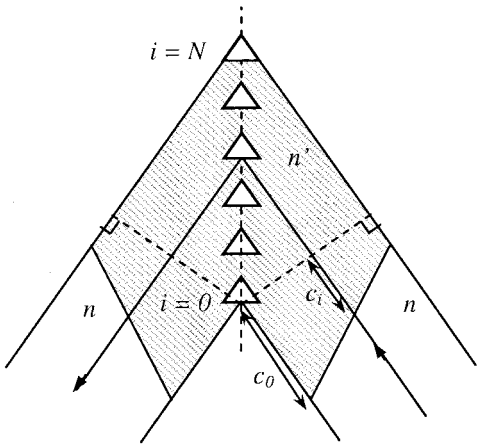

Fig. 5. Shallow-etch birefringence compensation. N is the number of grating elements, n is the effective index of the slab region, and n' is the effective index of the shallow-etched region (shaded).

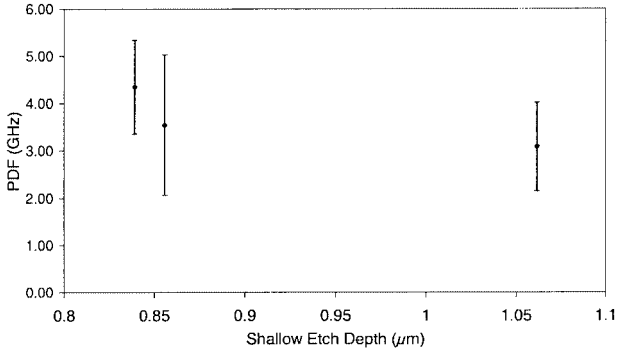

Fig. 6. PDF values for 100-GHz channel-spacing devices with shallow-etch birefringence compensation.

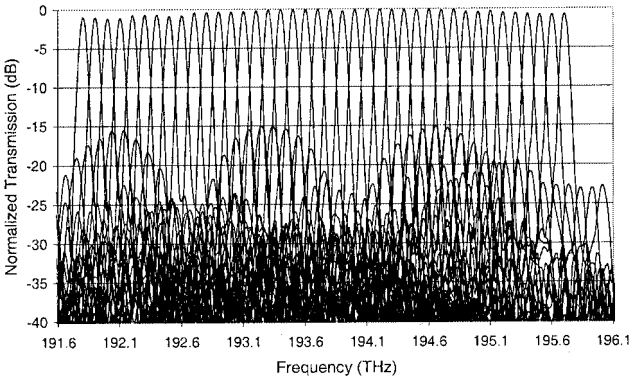

Fig. 7. Normalized channel spectra for PDF compensated 40-channel 100-GHz channel-spacing device.

100-GHz channel-spacing devices were fabricated by wet etching the compensation region: values of 0.8 and 1.1 μm etch were targeted. Averaged PDF results for several devices measured from three wafers are shown in Fig. 6. The actual etch depth was measured using a surface profiler. The results indicate that a significant improvement in PDF was obtained. However, there was a penalty in crosstalk and excess loss, although the PDL was found to be comparable to a device without the compensator.

Fig. 7 shows the normalized spectra. Significant side peaks have been introduced that limit the nonadjacent crosstalk to

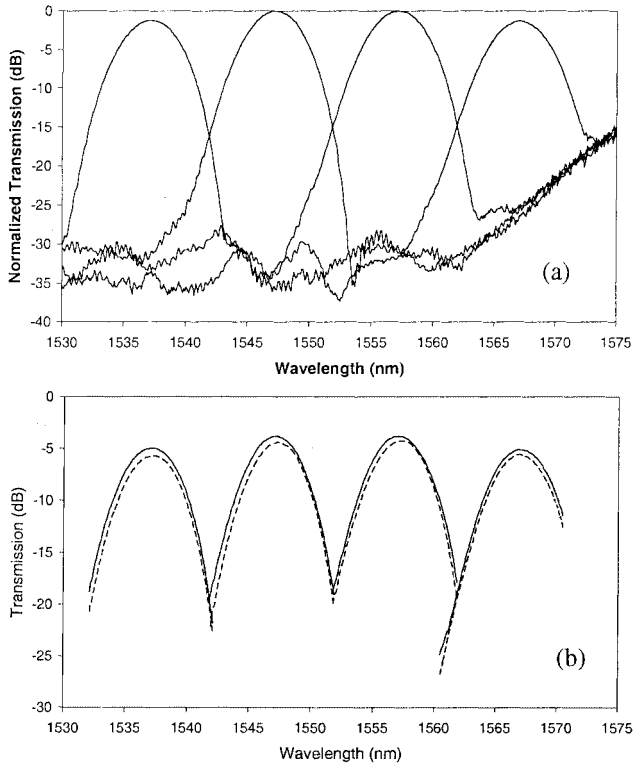

Fig. 8. Spectra for CWDM four-channel 10-nm channel-spacing devices. (a) Normalized spectra. (b) Minimum and maximum polarization spectral envelopes, showing on-chip loss.

15 dB. The origin of these side peaks is likely to be related to the excitation of higher order slab modes. The loss was up to 7 dB higher than for the devices without birefringence compensation. This was greater than the 3-dB expected based on the loss calculated for the interface with the compensation region using a simple one-dimensional overlap model. Further development of this technique should yield significant improvements in performance; one possible method to reduce the loss and crosstalk penalty is to use a multiple etch step at the interface to the compensation region.

B. CWDM Devices

The silicon reflection-type demultiplexers discussed in this paper are particularly suited to wider channel-spacing coarse wavelength-division multiplexing (CWDM) applications. The intrinsic PDF for these devices of 22 GHz is small compared to the clear-channel bandwidths anticipated for many CWDM applications, so birefringence compensation may not be required. This makes it substantially more straightforward to produce high-performance devices in terms of loss and crosstalk. Further, the fundamentally compact nature of these devices and the degree of control over the direction of the beam emerging from the demultiplexer element using reflection enables very efficient use of wafer area. The possibilities for denser integration are further enhanced by the fact that much of the area occupied by the demultiplexer consists of slab waveguide, so that propagating beams may be made to cross over with zero loss.

To demonstrate the potential use of these demultiplexers for wider channel spacing, a four-channel 10-nm channel-spacing

device was fabricated. The chip dimensions were $15 \times 1.5\ \text{mm}^2$ for a 250-μm output spacing. However, most of the chip area is taken up by the output waveguide fanout: the chip area occupied by the demultiplexer itself was less than $1\ \text{mm}^2$.

Fig. 8 shows measured transmission spectra from a typical device. The on-chip loss of this device was 5 dB for center channels, and the PDL was less than 0.6 dB.

Silicon has been demonstrated to be an excellent platform for the production of integrated optical devices using hybridized laser and detector elements [10]. Combining this capability with the extremely compact and high-performance demultiplexer devices discussed in this paper opens up further possibilities for applications in the CWDM domain.

IV. Conclusion

The results presented in this paper indicate that compact silicon reflection-based filters have the potential to meet the stringent performance specifications required for use in modern dense WDM and CWDM optical telecommunication systems.

Acknowledgment

The authors would like to thank M. Jackson and M. Seifouri for device fabrication.

References

[1] I. E. Day, S. W. Roberts, R. O'Carroll, A. Knights, P. Sharp, G. F. Hopper, B. J. Luff, and M. Asghari, "Single-chip variable optical attenuator and multiplexer subsystem integration," in *Proc. Optical Fiber Communication Conf. (OFC)*, Anaheim, CA, Mar. 2002, pp. 72–73.

[2] S. Janz, M. Pearson, B. Lamontagne, L. Erickson, A. Delâge, P. Cheben, D.-X. Xu, M. Gao, A. Balakrishnan, J. Miller, and S. Charbonneau, "Planar waveguide echelle gratings: An embeddable diffractive element for photonic integrated circuits," in *Proc. Optical Fiber Communication Conf. (OFC)*, Anaheim, CA, Mar. 2002, pp. 69–70.

[3] E. S. Koteles, "Integrated planar waveguide demultiplexers for high density WDM applications," in *Wavelength Division Multiplexing: A Critical Review*, L. S. Lome and R. T. Chen, Eds. Bellingham, WA: SPIE Optical Engineering Press, 1999, pp. 3–32.

[4] S. M. Ojha, G. H. B. Thompson, C. G. Cureton, G. B. Rogers, S. J. Clements, M. Asghari, and I. H. White, "Demonstration of low loss integrated InGaAsP/InP demultiplexer device with low polarization sensitivity," *Electron. Lett.*, vol. 29, pp. 805–807, Apr. 1993.

[5] M. Cowlin, M. Owen, I. H. White, and R. V. Penty, "Polymeric wavelength division multiplexer," *Electron. Lett.*, vol. 35, pp. 1464–1465, 1999.

[6] C. N. Morgan, I. H. White, and R. V. Penty, "Improved performance of compact silica 2DIO wavelength filters," in *Proc. Integr. Phot. Research (IPRC)*, Vancouver, BC, Canada, July 2002.

[7] A. Yariv, *Optical Electronics*. New York: Harcourt Brace Jovanovich, 1991, pp. 47–48.

[8] I. E. Day, I. Evans, A. P. Knights, G. F. Hopper, S. W. Roberts, J. Johnston, S. Day, B. J. Luff, H. K. Tsang, and M. Asghari, "Tapered silicon waveguides for low insertion loss highly-efficient high-speed electronic variable optical attenuators," in *Optical Fiber Communication Conf. (OFC)*, Atlanta, CA, Mar. 2003.

[9] J.-J. He, E. S. Koteles, B. Lamontagne, L. Erickson, A. Delâge, and M. Davies, "Integrated polarization compensator for WDM waveguide demultiplexers," *IEEE Photon. Technol. Lett.*, vol. 11, pp. 224–226, Feb. 1999.

[10] T. Bestwick, "ASOC—A silicon-based integrated optical manufacturing technology," in *Electron. Components Technol. Conf.*, Seattle, WA, May 1998, pp. 566–571.

B. J. Luff, photograph and biography not available at the time of publication.

V. Tsatourian, photograph and biography not available at the time of publication.

P. A. L. Stopford, photograph and biography not available at the time of publication.

S. W. Roberts, photograph and biography not available at the time of publication.

J. P. Drake, photograph and biography not available at the time of publication.

S. A. Fuller, photograph and biography not available at the time of publication.

M. Asghari, photograph and biography not available at the time of publication.